Nonlin. Processes Geophys., 16, 151–157, 2009
www.nonlin-processes-geophys.net/16/151/2009/

Nonlinear Processes in Geophysics

Modeling nonlinear compressional waves in marine sediments

B. E. McDonald

US Naval Research Lab, Washington DC, 20375, USA

Received: 31 October 2008 – Revised: 2 February 2009 – Accepted: 2 February 2009 – Published: 26 February 2009

Abstract. A computational model is presented which will help guide and interpret an upcoming series of experiments on nonlinear compressional waves in marine sediments. The model includes propagation physics of nonlinear acoustics augmented with granular Hertzian stress of order 3/2 in the strain rate. The model is a variant of the time domain NPE (McDonald and Kuperman, 1987) supplemented with a causal algorithm for frequency-linear attenuation. When attenuation is absent, the model equations are used to construct analytic solutions for nonlinear plane waves. The results imply that Hertzian stress causes a unique nonlinear behavior near zero stress. A fluid, in contrast, exhibits nonlinear behavior under high stress. A numerical experiment with nominal values for attenuation coefficient implies that in a water saturated Hertzian chain, the nonlinearity near zero stress may be experimentally observable.

1 Introduction

Explosions in the ocean produce shock waves which may transmit nonlinear compressional and shear waves to the seafloor. The propagation of nonlinear compressional waves in the seafloor is of interest because of their effect upon small buried structures such as mines and cables. Shear waves are of less concern to buried structures in the seafloor because (a) they arrive later than compressional waves and (b) their magnitude is limited by media failures. The temporal separation of first arrivals from compressional and shear waves also allows great theoretical simplification in the study of the compressional first arrival. This paper presents a nonlinear compressional wave model for the seafloor and illustrates with analytic solution and numerical simulation some novel behavior which might be realized in a saturated granular medium. The results presented here will help guide a planned series of experiments using nonlinear sources, and the experiments will be used to calibrate and verify the model.

The seafloor as a propagation medium is made up of fluid and granular components. The bulk modulus of the medium is comparable to or greater than that of water, and thus explosive waveforms are quickly reduced to weak nonlinearity as defined by either overdensity or strain rate. The fluid has a stress- strain relation amenable to series expansion for small strain rate, while the granular stress-strain relation involves fractional powers 3/2, 5/2 in the strain rate (Makse et. al, 2004).

Compressional waves with small but finite nonlinearity (e.g. overdensity) are described by the equations of nonlinear acoustics (Beyer, 1997), according to which nonlinearities develop at a rate proportional to the nonlinearity coefficient β defined as

$$\beta \equiv 1 + \frac{\rho}{2c^2}\frac{\partial^2 p}{\partial \rho^2}\Big|_0 , \tag{1}$$

where ρ is density, c is compressional wave speed, p is pressure (or more generally normal stress) and subscript 0 refers to evaluation in the ambient state. Values for β in air and water (both fluid media) are approximately 1.2 and 3.5, respectively. In granular or consolated solids, however, the values are much higher (Ostrovsky, 1991): 800 for marble, and $10^2 - 10^3$ for dry clay sediments. Recent theoretical results (Donskoy et al., 1997) agree with values such as these for granular media.

Very little experimental work has been published on nonlinear compressional waves in saturated marine sediment since the 1970's. Early work (Bjorno, 1977; Hovem, 1979) reported only modest values for the nonlinearity coefficient, finding values in the range approximately 5.7 to 7.0 (in the notation of the cited works, β=1+B/2A). The experimental method used was to measure the linear sound speed of the medium as a function of applied pressure. The shortfall of this method is that measurements are taken with linear waves in a quiescent medium. The modest values found are consistent with expressions for a quiescent mixture of quartz and

Correspondence to: B. E. McDonald
(mcdonald@ccs.nrl.navy.mil)

water in the absence of intergranular stresses and flows. In the case of a finite amplitude wave, however, one may expect shock formation, granular stresses, and highly contorted intergranular flow of finite amplitude.

Experiments with lattices of glass beads have confirmed an effective medium description in agreement with Hertz-Mindlin theory in which stress is related to the 3/2 power of strain (Vilicky and Caroli, 2002). In particular, the compressional wave speed increases as the 1/6 power of ambient pressure after the beads are sufficiently compacted. In marine sediments, a compressional wave will increase granular stresses if the bulk modulus of the grain material (e.g. quartz for sand) is higher than that of the fluid between the grains. This is especially true if the fluid contains bubbles and is thus more compressible.

We propose an effective medium model for saturated sediments, with fluid stresses of first and second order in the strain rate, and Hertzian intergranular stresses of order 3/2 and 5/2 (Makse et. al, 2004). The 3/2 order term reflects the stress-strain relation for elastic grains in contact (Landau and Lifschitz, 1959), while the 5/2 order term allows increasing number of contacts per grain with increasing stress. Wave attenuation due to shear and intergranular flow will be added separately.

Coefficients for the effective medium model will be determined in upcoming laboratory and field experiments (McDonald, 2008). Some surprising features of the Hertzian stress- strain relation to be illustrated below are (1) the most evident nonlinearity (shock formation) occurs preferentially near low stress points; and (2) continuous profiles can generate shock discontinuities instantaneously (as opposed to shock formation after a steepening period). It is not at all clear if these features can be seen in real sediments due to high attenuation and increasing grain contacts with increased stress.

The presence of a 3/2 order Hertzian stress term in an effective medium description of saturated sediment poses two interesting challenges to the theory of nonlinear acoustics: (1) the lowest order nonlinearity is no longer quadratic and (2) the Taylors' series expansion of the effective equation of state to second order fails at zero stress.

2 An effective medium model

We propose the following theoretical model, which is a variant of the nonlinear progressive wave equation (NPE), a paraxial approximation to the Euler equations of fluid dynamics developed for investigating weak shock propagation in refractive fluid media (McDonald and Kuperman, 1987):

$$D_t\rho' = -\frac{1}{2c_0}\partial_x\left[p(\rho') + c_0^2(\rho'^2/\rho_0 - \rho')\right] - \frac{c_0}{2}\int_\infty^x \nabla_\perp^2\rho' dx, \quad (2)$$

where prime denotes deviation from ambient value (subscript zero), x is the primary wave propagation direction, and $\nabla_\perp^2 \equiv \partial_y^2 + \partial_z^2$ is the Laplacian transverse to x. The operator $D_t \equiv \partial_t + c_0\partial_x$ is the time derivative in a wave-following frame moving at speed c_0 in the x direction. This model is appropriate for media which support acoustic waves in the ambient state. For this reason it applies to saturated sediment, but not to dry unconsolidated granular media which do not support acoustic waves at zero stress. The $x-$integration path in (2) begins in the quiescent medium ahead of the wave where ρ' and its derivatives are zero. Error terms in (2) are $O(\rho'^3,\ \rho'^2\theta^2)$, where θ is the wavenormal angle with respect to x. For this reason it is sufficient to use an adiabatic equation of state $p(\rho')$ since weak shock heating is cubic in shock amplitude.

The effective medium equation of state $p(\rho')$ is taken to be of the form

$$p(\rho') = p_0 + \rho_0 c_0^2\left(\left(\frac{\rho'}{\rho_0}\right) + (\beta_0 - 1)\left(\frac{\rho'}{\rho_0}\right)^2\right) + \\ + K_{3/2}\max\left(0,\ \frac{\rho'}{\rho_0}\right)^{3/2} + K_{5/2}\max\left(0,\ \frac{\rho'}{\rho_0}\right)^{5/2}. \quad (3)$$

The linear and quadratic terms in (3) are fluid stresses, and the fractional orders are granular stresses. Constants ρ_0, c_0, and β_0 are the bulk values for density, sound speed and nonlinearity coefficient for the water/grain mixture in the absence of grain contact, and are determined by elementary methods with knowledge of porosity of the mixture and density of the grain material. For spherical grains, the K constants are determined from expressions (Makse et. al, 2004) involving the porosity of the mixture, number of contacts per grain, grain radius and elastic moduli of the grain material. For sediments, however, the grain geometries and contact numbers vary, so that an experimental determination is required. The max function in (3) reflects that granular contacts can transmit only positive stress, not tension. When using (3) in the time domain model (2), the fractional order terms are evaluated as such numerically, in contrast to standard nonlinear acoustics of fluids where the entire equation of state is expressed in power series.

Attenuation due to intergranular flow and shear between grains is observed to scale very nearly linearly with frequency (Buckingham, 2000), in contrast to laminar viscosity, which scales with frequency squared. It is empirically observed that the attenuation in sediments is of order 1 dB per wavelength. One might consider attempting to evaluate frequency-linear attenuation by Fourier transforming the wave profile, multiplying each component by its wavenumber times a constant proportional to the attenuation coefficient, and inverse transforming. This would, however, violate causality. To see this, consider a point x in the medium during the passage of a wave propagating to the right. Fourier transforms sum over the entire spatial domain, including the wave which has not yet reached x. Causality requires that the point x be affected only by the portion of the wave that has already passed over it. The algorithm to be presented below may be represented as a convolution with a one-sided kernel,

with no contribution from the wave to the left of the point x. (One could in principle use fast Fourier transform methods to evaluate the one-sided convolution more rapidly than a straightforward numerical sum.)

A causality preserving algorithm for frequency-linear attenuation is the following, which is added as a separate step to Eq. (2):

$$D_t^+\rho'(x,\,y,\,z,\,t) = \frac{\ln 10}{20\pi^2}\alpha c_0\partial_x\int_0^\infty \frac{\rho'(x+\xi,\,y,\,z,\,t)}{\delta+\xi}d\xi\,, \quad (4)$$

where α is the attenuation coefficient expressed in dB per wavelength. The integration variable ξ is a spatial coordinate which scans forward over the entire profile of the wave which has already passed over x. The coefficient $\ln 10/(20\pi^2)$=.01166 is determined by substituting trial sinusoids into (4) and comparing the result with the exponential integral function E_1 in the limit of small argument. The constant δ is a minimum scale size smaller than any wavelength of interest (Eq. 4 results in dB per wavelength values within 10% of α for wavenumbers k such that $k\delta\leq$.06). The causal nature of (4) is reflected in the one sided integral, so that a point in the medium is affected by only the portion of the wave that has already passed over it.

2.1 Nonlinear plane waves

In three dimensions, Eq. (2) (absent attenuation) admits similarity solutions $\rho'(\mathbf{r},\,t)=\rho'(\mathbf{r}/t)$, a property inherited from the Euler equations. At large propagation distances, these waves approach nonlinear plane waves which are stable to arbitrary three dimensional perturbation (McDonald, 2006). In one dimension, Eq. (2) yields insight into the effects of Hertzian nonlinearity via similarity solutions and/or solutions obtained through the method of characteristics. The one dimensional version of (2) is

$$\rho'_t = -f(\rho')\partial_x\rho' \quad (5)$$

where subscript t denotes the moving frame time derivative D_t, and

$$f(\rho') = \frac{1}{2c_0}\left(\frac{\partial p}{\partial\rho'} + c_0^2(2\rho'/\rho_0 - 1)\right) \quad (6)$$

f is the signal propagation speed in excess of c_0 to the same order accuracy as (2). If an equation of state $p(\rho')$ is known, then $f(\rho')$ is known and a similarity solution $\rho'(x/t)$ may be obtained (McDonald, 2006) by solving $f(\rho')=x/t$. More generally, the complete evolution from an initial condition in (5) may be found by the method of characteristics:

$$\rho'(x,\,t) = g\left(x - tf(\rho')\right), \quad \text{where} \quad g(x) = \rho'(x,\,0). \quad (7)$$

Taking the x derivative of (7) and bringing $\partial_x\rho'$ to the left side gives

$$\partial_x\rho'(x,\,t) = \frac{\rho'_x(x_r,\,0)}{1 + t\rho'_x(x_r,\,0)\left(\frac{\partial^2 p}{\partial\rho'^2} + \frac{2c_0^2}{\rho_0}\right)/2c_0} \quad (8)$$

where $\rho'_x(x_r,\,0)$ refers to $\partial_x\rho'$ evaluated at t=0, $x_r=x-tf(\rho'(x,\,t))$. Note from (6) that $f(0)$=0, so continuous zeros (as opposed to shock jumps with zero on one side of the shock) of ρ' remain fixed in the moving frame. Consider a continuous zero which occurs at $x=x_z$ and t=0. Then (6), (8), and (1) give the wave slope at the zero at later times as

$$\rho'_x(x_z,\,t) = \frac{\rho'_x(x_z,\,0)}{1 + c_0t\beta\rho'_x(x_z,\,0)/\rho_0}\,. \quad (9)$$

Equation (9) makes the remarkable statement that if β diverges at a continuous zero, the wave slope is immediately forced to zero or infinity (i.e. shock formation occurs) depending on the sign of the wave slope. This is to be contrasted with the case for finite β, where shock formation time is $t_s^{-1}=-c_0\beta\rho'_x(x_z,\,0)/\rho_0$ when $\rho'_x(x_z,\,0)<0$.

What conditions could lead to divergent β? Consider adding Hertzian stress to fluid normal stress $p=p_f+E'(\rho'/\rho_0)^{3/2}$, where p_f is fluid pressure and E' is proportional to the Young's modulus of the grain material. Then β from (1) contains a term proportional to $(\rho'/\rho_0)^{-1/2}$, which diverges in the ambient state ρ'=0. This is one reason for the extremely high values of β for granular materials cited earlier.

2.2 Instantaneous shock formation

To illustrate the consequences of divergent nonlinearity coefficient β, consider the following model problem which yields a convenient analytic solution:

$$u_t = -\frac{2}{3}\left(u^{3/2}\right)_x = -u^{1/2}u_x\,, \quad (10)$$

where x, t and u are dimensionless. Equation (10) is a dimensionless surrogate for Eq. (5) to lowest order where ambient density and sound speed are normalized to unity. In (10) u plays the role of the density perturbation, and $u^{3/2}$ plays the role of overpressure. Then (1) shows that β diverges as $u\to 0$. For an initial condition with positive slope at a continuous zero we take $u(x,\,0)=\max(x,\,0)$. Then (10) has solution

$$u(x\geq 0,\,t) = x + \frac{t^2}{2}\left[1 - \sqrt{1 + 4x/t^2}\right] \quad (11)$$

as illustrated in Fig. 1a. One finds from (11) that $u_x(0,\,t)$=0 for any $t>0$, so that the profile is flattened instantaneously at x=0.

For an initial condition with negative slope at a continuous zero we take $u(x,\,0)=\max(-x,\,0)$. The analytic solution with a continuous zero arising from this initial condition becomes double valued for any $t>0$:

$$u(x,\,t) = -x + \frac{t^2}{2}\left[1 \pm \sqrt{1 - 4x/t^2}\right] \quad (12)$$

The physically relevant solution for this initial condition is found by resolving the double value into a shock using the

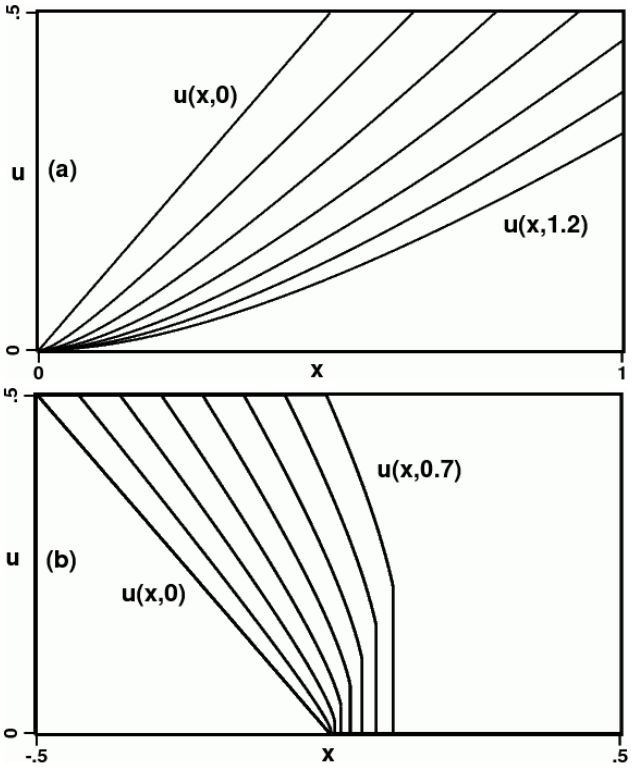

Fig. 1. **(a)** Analytic solution (11) to Eq. (10) for ascending initial condition illustrating instantaneous flattening at x=0. Curves are plotted at equal time increments. **(b)** Analytic solution (14) for descending initial condition and resulting instantaneous shock formation.

equal area rule, or equivalently by imposing the Rankine Hugoniot condition for the shock location:

$$\frac{dx_s}{dt} = [\frac{2}{3}u^{3/2}]/[u] \tag{13}$$

where the bracket indicates the discontinuity across the shock and subscript s denotes evaluation just behind the shock. The result is x_s=$2t^2/9$, with jump u_s=$4t^2/9$. Thus the single valued solution is

$$u(x < x_s,\, t) = -x + \frac{t^2}{2}\left[1 + \sqrt{1 - 4x/t^2}\right] \tag{14}$$

and u=0 for x>x_s. This solution is illustrated in Fig. 1b, and shows that a discontinuity begins to grow from zero immediately for t>0, increasing quadratically with time.

The approach toward linear behavior as wave amplitude approaches zero is illustrated by replacing $u \rightarrow \epsilon u$ in (10) with $\epsilon \rightarrow 0$. Then the timescale for development of initially infinitessimal shocks increases as $\epsilon^{-1/2}$, and becomes infinite. Thus, linear behavior is retained as the shocks remain infinitessimal in amplitude for any finite time.

In a series of experiments to be carried out during 2009–2011 (McDonald, 2008), we will look for evidence of behaviors illustrated in Fig. 1. The series will include laboratory experiments with a focused spark source similar to a lithotripter (Bailey et al., 1998), a focused laser, and a field experiment with an air gun. It is quite possible that conditions for instantaneous shock formation may not be realized if the fluid between the grains is not sufficiently compressed, if the grains increase contact numbers during compression, or if the effect is suppressed by attenuation.

2.3 Addition of frequency-linear attenuation

We will illustrate the effect of attenuation on a Hertzian medium by a numerical experiment combining Eqs. (4) and (5). The resulting equation,

$$\rho'_t = -f(\rho')\partial_x\rho' + \alpha\frac{\ln 10}{20\pi^2}c_0\partial_x\int_0^\infty \frac{\rho'(x+\xi,t)}{\delta+\xi}d\xi, \tag{15}$$

will be cast in nondimensional form for comparison with the analytic solution (14) with appropriate initial conditions. Since we are interested in modeling the first arriving and strongest wave, we will consider fluid and grain motions corresponding to the fast wave of Biot theory (Buckingham, 2000). In this mode, fluid and grains move nearly in phase (as opposed to the highly damped slow wave where they are out of phase).

To approximate an upper limit on granular stress we consider a Hertzian chain of equal sized spheres, with water between the spheres. When two identical elastic spheres are forced together, the stress- strain relation is (Landau and Lifschitz, 1959)

$$F = \frac{\sqrt{2}}{3}\frac{E}{1-\sigma^2}h^{3/2}R^{1/2}, \tag{16}$$

where F is the normal force between the two spheres, h is the decrement in sphere center separation, R is the sphere radius, E is the grain material Young's modulus, and σ is Poisson's ratio. Such a Hertzian chain might be realized in the laboratory by placing spheres in a water filled pipe whose radius is slightly larger than R. The normal stress averaged over a test plane perpendicular to the chain axis will be the fluid pressure plus the granular force (16) divided by the chain's cross section πR^2.

Consider now unidirectional compaction of the chain by a compressional wave whose wavelength is much larger than the grain radius. The grain material (e.g. quartz) has a much higher bulk modulus than water, so the grains retain nearly constant volume while being easily deformed (Eq. 16 has zero derivative at zero strain h). The average strain rate and compressibility are thus that of the water, and we may take $h \simeq 2R\rho'/\rho_0$, where ρ_0 is the density of the water/grain chain at zero stress, ρ_0=$(\rho_w$+$2\rho_g)/3$, subscripts w and g refer to water and grain material, and ρ' is the deviation of average density from ρ_0. As a result of the water filled Hertzian chain

having the same unidirectional compressibility of water, one has $\rho_0 c_0^2 = \rho_w c_w^2$.

From (3) and (16) we construct an equation of state for the water filled Hertzian chain, retaining only the lowest order nonlinearity:

$$p(\rho') = p_0 + \rho_0 c_0^2 \frac{\rho'}{\rho_0} + K_{3/2} \left(\frac{\rho'}{\rho_0}\right)^{3/2} \tag{17}$$

where

$$K_{3/2} = \frac{4}{3\pi} \frac{E}{1-\sigma^2} \tag{18}$$

From (6), (15) and (17) we have to lowest order

$$f(\rho') = \frac{1}{\pi \rho_0 c_0} \frac{E}{1-\sigma^2} \left(\frac{\rho'}{\rho_0}\right)^{1/2} . \tag{19}$$

The next step is to nondimensionalize Eq. (15) using (19) so that the term involving $f(\rho')$ coincides with the right side of Eq. (10). To do this we substitute $x = x_0 x'$ and $t = t_0 t'$, where the primed variables are dimensionless, and x_0, t_0 are dimensional length and time scales to be specified later.

Then we set $u(x, t) = b\rho'/\rho_0$, where b is a dimensionless constant. The result is (after dropping primes from x' and t')

$$\begin{aligned} u_t = &- \tfrac{t_0}{x_0 c_0} \tfrac{3K_{3/2}}{4\rho_0} b^{-1/2} u^{1/2} u_x \\ &+ \alpha \tfrac{c_0 t_0}{x_0} \tfrac{\ln 10}{20\pi^2} \partial_x \textstyle\int_0^\infty \tfrac{u(x+\xi, t)}{\delta+\xi} d\xi . \end{aligned} \tag{20}$$

In (20) we have also nondimensionalized ξ and δ by x_0. The scale size inherent to the problem is the grain radius. We are free to choose x_0 to be a large number times the grain radius, so that an effective medium description may be applicable. Then a unit interval in x will represent many times the grain size. The corresponding time scale is $t_0 = x_0/c_0$, so the first term on the right side of (20) agrees with the RHS of (10) when

$$b = \left(\frac{3K_{3/2}}{4\rho_0 c_0^2}\right)^2 = \left(\frac{1}{\pi \rho_0 c_0^2} \frac{E}{1-\sigma^2}\right)^2 \tag{21}$$

and (20) becomes

$$u_t = -u^{1/2} u_x + \alpha \frac{\ln 10}{20\pi^2} \partial_x \int_0^\infty \frac{u(x+\xi, t)}{\delta+\xi} d\xi . \tag{22}$$

3 Numerical solution

To expedite numerical calculations, we replace the integral in (22) with a more rapidly converging one obtained as follows. The integral term in (22) may be written as

$$\begin{aligned} \partial_x \textstyle\int_0^\infty \tfrac{u(x+\xi, t)}{\delta+\xi} d\xi &= \textstyle\int_0^\infty \tfrac{\partial_x u(x+\xi, t)}{\delta+\xi} d\xi \\ &= \textstyle\int_0^\infty \tfrac{\partial_\xi u(x+\xi, t)}{\delta+\xi} d\xi . \end{aligned} \tag{23}$$

The last expression may be integrated by parts, and (22) becomes

$$u_t = -u^{1/2} u_x + \alpha \frac{\ln 10}{20\pi^2} \left(\int_0^\infty \frac{u(x+\xi, t)}{(\delta+\xi)^2} d\xi - \frac{u(x, t)}{\delta} \right) , \tag{24}$$

where values at infinity are taken to be zero.

To evaluate b in (21) we take $\rho_0 c_0^2 = 2.25$ GPa (the bulk modulus of water), and moduli values for quartz: $E = 95.3$ GPa, $\sigma = .0588$ (Carmichael, 1982). The result is $b = 183.0$. In planned experiments using impulsive nonlinear sources (lithotripter, air gun, and focused laser), we first consider the lithotripter, which is likely to produce the highest amplitude. Peak pressures in experiments with lithotripters are of order 40 MPa in pulses of order 1 μs duration (Bailey et al., 1998), so that from (17) we estimate $\rho'_{\max}/\rho_0 \simeq .0071$, and the dimensionless value $u_{\max} \simeq 1.30$.

Equation (24) has been integrated numerically with the initial condition $u(x, 0) = \max(-x, 0)$ on the interval $(-5, 5)$ on a grid of 501 points of equal spacing δx, and 1121 evenly spaced time steps. The value of δ in (24) was $0.2\delta x$. The method used for the nonlinear term is a monotonicity preserving second order upwind scheme (McDonald and Ambrosiano, 1984), and an explicit forward difference scheme for the integral. Figure 2 shows the integration for three α values (0, 1, 2) dB/wavelength. The points are the shock jump from the analytic solution (14); the $\alpha = 0$ case illustrates the shock capturing accuracy of the numerical scheme. As α is increased, the solution becomes more attenuated, but still shows signs of rapid shock formation. The relevant solution for $u_{\max} = 1.30$ is found in the lower third of each panel.

We have not so far specified the time and length scales t_0 and x_0. Before doing this, we can state that the sound speed of water filled Hertzian chain is $c_0 = c_w \sqrt{\rho_w/\rho_0}$ as a result of the chain's bulk modulus in unidirectional strain being that of water for small strain. Taking $\rho_g = 2650$ kg/m^3, $\rho_0 = (\rho_w + 2\rho_g)/3 = 2100$ kg/m^3, and $c_w = 1500$ m/s, we have $c_0 = 1035$ m/s. If we take t_0 to be the 1μsec pulse duration of the lithotripter experiment cited above (Bailey et al., 1998), then we find $x_0 = c_0 t_0 = 1.035$ mm. The axial extent of the simulation of Fig. 2 then becomes 10.35 mm, large enough for an effective medium description if the grain diameters are less than 1 mm.

One of the planned experiments will use an airgun, which produces pulses of duration $t_0 \simeq 10$ ms. Airguns emit air at an initial pressure of about 2000 psi $\simeq 14$ MPa. If the pulse is captured in a pipe to limit spherical spreading loss, and if the above parameters for the water filled Hertzian chain are used, one would have $u_{\max} = 0.567$, and $x_0 = 10.35$ m. Thus the dimensionless span of Fig. 2 becomes 103.5 m. While it would be impractical to construct a Hertzian chain of order 100 m length, a modest length of 3 m might be practical using fairly large glass spheres. It would occupy a span of length 0.29 in Fig. 2. This could be sufficient to observe evidence of rapid shock formation in the presence of nominal attenuation val-

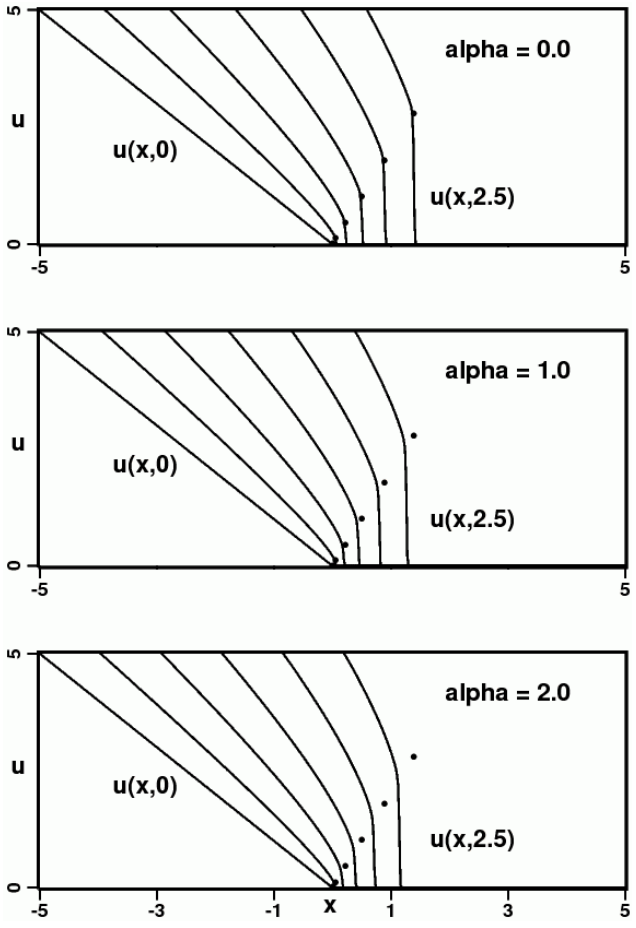

Fig. 2. Numerical integration of (24) for increasing values of attenuation coefficient α (dB per wavelength). Curves in each panel are plotted at equal intervals of dimensionless time from t=0 to t=2.5. The points plotted show the shock jump $x_s=2t^2/9$, $u_s=4t^2/9$ in the analytic solution (14).

ues in a water filled Hertzian chain using an air gun source. (No data are yet available for our laser source.)

To contrast the behavior illustrated in Fig. 2 with the behavior of a fluid subject to quadratic nonlinearity, we note that to lowest order the signal speed in excess of c_0 in a fluid is $\beta c_0 \rho'/\rho_0$. Thus we replace (10) with the nondimensionized equation

$$u_t = -uu_x, \tag{25}$$

where $u=\beta\rho'/\rho_0$. Equation (24) may be recognized as the inviscid Burgers equation. The solution arising from (24) and (7) with initial condition $u(x,\,0)=\max(-x,\,0)$ is then $u(x,\,t)=\max(-x,\,0)/(1-t)$. The nondimensional shock formation time for comparison with Fig. 2 is t_s=1. Thus shock formation is evident in the Hertzian chain example of Fig. 2 before the onset of a shock in an equivalent nondimensional fluid problem with quadratic nonlinearity. Restoring dimensions to this simple fluid problem, one has

$$\frac{\rho'(x,\,t)}{\rho_0} = \frac{\max(-x,\,0)}{c_0\beta(t_0 - t)}, \tag{26}$$

so that $\rho'_x(0,\,t)=\rho'_x(0,\,0)/(1+\beta c_0 t\rho'_x(0,\,0)/\rho_0)$ as stated earlier.

4 Conclusions

We have proposed an effective medium description and propagation model for nonlinear compressional waves in saturated marine sediments in Eqs. (2–4), which will be calibrated against future experiments with finite amplitude nonlinear sources. Analytic and numerical nonlinear plane wave solutions suggest that when the order 3/2 Hertzian nonlinearity is present, it can result in divergent values of the nonlinearity parameter β at zero stress, with shock discontinuities forming more rapidly than in a fluid with quadratic nonlinearity.

In the absence of attenuation, we have shown in Eq. (8) that where the nonlinearity coefficient diverges, either (1) the wave slope at a continuous zero is forced to zero immediately, or (2) that a shock discontinuity begins immediately, depending on whether the slope is ascending or descending. These behaviors have been confirmed in analytic solutions, Eqs. (10–14).

When attenuation is present, the numerical experiment shown in Fig. 2 indicates that it might be possible to observe signs of rapid shock formation in a water filled Hertzian chain, with attenuation of order one dB per wavelength, as common to marine sediments.

Acknowledgements. Work supported by the US Office of Naval Research.

Edited by: R. Grimshaw
Reviewed by: two anonymous referees

References

Bailey, M. R., Blackstock, D. T., Cleveland, R. O., and Crum, L. A.: Comparison of electrohydraulic lithotripters with rigid and pressure-release ellipsoidal reflectors, I. Acoustic fields, J. Acoust. Soc. Am., 104, 2517–2524, 1998.

Beyer, R. T.: Nonlinear Acoustics, Acoustical Society of America, Huntington, NY, 435 pp., 1997.

Bjorno, L.: Finite amplitude wave propagation through water-saturated marine sediments, Acustica, 38, 195–200, 1977.

Buckingham, M. J.: Wave propagation, stress relaxation, and grain-to-grain shearing in saturated, unconsolidated marine sediments, J. Acoust. Soc. Am., 108, 2796–2815, 2000.

Carmichael, R. S.: Practical handbook of physical properties of rocks, CRC Press, Boca Raton FL, v. II, 694–715, 1982.

Donskoy, D. M., Khashanah, K., and McKee T. G.: Nonlinear acoustic waves in porous media in the context of Biot's theory, J. Acoust. Soc. Am., 102, 2521–2528, 1997.

Hovem, J.: The nonlinearity parameter of saturated marine sediments, J. Acoust. Soc. Am., 66, 1463–1467, 1979.

Landau, L. D. and Lifschitz, E. M.: Theory of Elasticity, Addison-Wesley, 30–35, 1959.

Makse, H., Gland, N., Johnson, D., and Schwartz, L: Granular packings: nonlinear elasticity, sound propagation, and collective relaxation dynamics, Phys. Rev. E, 70, 061302, 1–19, 2004.

McDonald, B. E. and Ambrosiano, J.: High order upwind flux correction methods for hyperbolic conservation laws, J. Comp. Phys., 56, 448–460, 1984.

McDonald, B. E. and Kuperman W. A.: Time domain formulation for pulse propagation including nonlinear behavior at a caustic, J. Acoust. Soc. Am., 81, 1406–1417, 1987.

McDonald, B. E.: Probing the seafloor with nonlinear compressional waves, Geophys. Res. Abstr., 10, EGU2008-A-02822, 2008.

McDonald, B. E.: Stability of Self-Similar Plane Shocks with Hertzian Nonlinearity, J. Acoust. Soc. Am., 120, 3503–3508, 2006.

Ostovsky, L. A.: Wave processes in media with strong acoustic nonlinearity, J. Acoust. Soc. Am., 90, 3332–3337, 1991.

Velicky, B. and Caroli, C.: Pressure dependence of the sound velocity in a two-dimensional lattice of Hertz-Mindlin balls: Mean-field description, Phys. Rev. E, 65, 021307, 1–14, 2002.